Paramagnetic fluctuations of the magnetocaloric compound $MnFe_4Si_3$

N. Biniskos [1,2,*] K. Schmalzl [3] J. Persson,[4] and S. Raymond [5,†]

[1] *Charles University, Faculty of Mathematics and Physics, Department of Condensed Matter Physics, Ke Karlovu 5, 121 16 Praha, Czech Republic*

[2] *Forschungszentrum Jülich GmbH, Jülich Centre for Neutron Science at MLZ, Lichtenbergstrasse 1, D-85748 Garching, Germany*

[3] *Forschungszentrum Jülich GmbH, Jülich Centre for Neutron Science at ILL, 71 Avenue des Martyrs, F-38000 Grenoble, France*

[4] *Forschungszentrum Jülich GmbH, Jülich Centre for Neutron Science (JCNS-2), JARA-FIT, D-52425 Jülich, Germany*

[5] *Université Grenoble Alpes, CEA, IRIG, MEM, MDN, F-38000 Grenoble, France*

(Received 29 July 2024; accepted 3 February 2025; published 18 February 2025)

An inelastic neutron scattering technique is employed to investigate the paramagnetic spin dynamics in a single-crystalline sample of the magnetocaloric compound $MnFe_4Si_3$. In the investigated temperature range, $1.033 \times T_C$ to $1.5 \times T_C$, where T_C is the Curie temperature, the spin fluctuations are well described by the ferromagnetic Heisenberg model predictions. Apart from the Heisenberg exchange, additional pseudodipolar interactions manifest through a finite long-wavelength relaxation rate that vanishes at the transition temperature ($T_C = 305$ K). Based on the characteristic extent of spin fluctuations in wave-vector and energy space, we determine that the nature of magnetism in $MnFe_4Si_3$ is localized above room temperature. This contrasts with the most celebrated Mn- and Fe-based magnetocaloric materials that are considered as itinerant magnets. The field dependence of the paramagnetic spectra shows a strong suppression of the quasielastic excitations, while a field-induced spin-wave mode appears at finite-energy transfers for a magnetic field of 2 T. This modification of the spectra suggests a decrease of magnetic entropy with applied magnetic field that finds echo in the magnetocaloric properties of the system.

DOI: 10.1103/PhysRevB.111.054424

I. INTRODUCTION

Magnetism in solids originates from the atomic magnetic moments, which are a consequence of the spin and angular momenta of the electrons. A magnetically ordered phase is described by the order parameter M (e.g., magnetization for a ferromagnet) that vanishes in the paramagnetic (PM) state. At finite temperature, thermal spin fluctuations mostly account for the reduction of M. Such fluctuations are enhanced near the transition temperature and persist in the PM state [1]. They manifest as a continuum of excitations in the wave-vector and energy ($\mathbf{q}$, E) space.

For several cubic ferromagnets (FM), the spin fluctuations around and above the Curie temperature (T_C) have been extensively investigated by inelastic neutron scattering (INS) measurements [2–10]. These reports retrieved properties about the temperature dependence of the q-dependent relaxation rate Γ_q and the inverse spin correlation length κ. At T_C, Γ_q follows the expression $\Gamma_q \propto Aq^z$, with z the dynamical exponent, while for $T > T_C$, $\kappa(T) = \kappa_0(T/T_C - 1)^\nu$, where κ_0 refers to the inverse spin correlation length at $T = 0$ K and ν is the usual critical exponent describing the divergence of the correlation length $\xi \sim \kappa^{-1}$ at T_C. The interest of such studies lies in the fact that when A and κ_0 are compared to T_C and the interatomic distance d^*, respectively, further insights about the nature of the magnetism of a material can be obtained. For localized magnetic systems, it is expected $A/T_C \approx 1$ and $d^*\kappa_0 \approx 1$, while for itinerant magnets, $A/T_C \gg 1$ and $d^*\kappa_0 \langle\langle 1$ [1,11]. These differences are due to the fact that the length scales are related to typical interatomic distances in localized magnetic systems and their energy scales are mainly controlled by the exchange interactions, to which T_C scales in a mean-field approach. In contrast to other parameters, characteristics of the electronic band structure and the Fermi surface need to be considered for itinerant systems. It is also worth mentioning that investigations of the spin fluctuations with INS have focused mainly on cubic FM, while similar studies for FM materials with lower crystal symmetries are scarce [12–14].

Hence, the extension of the spin fluctuations in momentum/energy space is a way to characterize the nature of magnetism in solids. Apart from being of fundamental interest for understanding the microscopic magnetism of a compound, the fluctuations can play an important role in macroscopic phenomena associated to a given magnetic functionality of a material. The appearance of significant spin fluctuations can be associated with large changes in the magnetic entropy of a system. Based on the Maxwell relations, it is known that any temperature dependence of the magnetization is connected to

*Contact author: nikolaos.biniskos@matfyz.cuni.cz

†Contact author: raymond@ill.fr

an entropy change when changing an external magnetic field. This effect is exerted for achieving sub-Kelvin temperatures through the adiabatic demagnetization of paramagnetic salts, and for magnetic refrigeration applications in daily life via the giant magnetocaloric effect (MCE) that is observed near room-temperature magnetic phase transitions [15].

Despite the numerous research articles that quantify the MCE in several magnetic materials using macroscopic measurements [15–17], such as heat capacity and magnetization, studies of the spin fluctuations and their relation to the MCE have only been discussed in a handful of systems with neutron spectroscopic studies, namely, in $MnFe_4Si_3$ [18], Mn_5Si_3 [19], (Mn, Fe)$_2$(P,Si) [20], $LaFe_{13-x}Si_x$ [21–23], and HoF_3 [24]. To this aim, we employ polarized INS measurements and unpolarized INS under magnetic field to probe the magnetization dynamics above T_C of the hexagonal metallic FM $MnFe_4Si_3$ and we propose links between the underlying temperature and magnetic field effects with the MCE.

In $MnFe_4Si_3$, a second-order phase transition from the PM state to the FM phase occurs near room temperature ($T_C = 305$ K) [18,25,26]. The material crystallizes in the hexagonal space group $P6_3/mcm$ [27,28]. Within the structure, the Wyckoff position (WP) 4*d* is occupied by Fe atoms surrounded by six Si atoms, while the WP 6*g* has a mixed occupancy of Fe-Mn (Fe occupancy ≈67%, Mn occupancy ≈33%). The magnetic moments on the WP 6*g* lie in the *ab* plane of the hexagonal symmetry with a magnitude of 1.5(2) μ_B, while no significant magnetic moment could be determined on the WP 4*d* [29].

II. EXPERIMENTAL DETAILS

A $MnFe_4Si_3$ single crystal (the same used in previous studies [18,30]) with mass of about 7 g and grown by the Czochralski method was oriented in the (a^*, c) scattering plane of the hexagonal symmetry. In this article, we use the hexagonal coordinate system and the scattering vector $\mathbf{Q}$ is expressed in $\mathbf{Q} = (Q_h, Q_k, Q_l)$ given in reciprocal lattice units (r.l.u.). The wave vector $\mathbf{q}$ is related to the momentum transfer through $\hbar\mathbf{Q} = \hbar\mathbf{G} + \hbar\mathbf{q}$, where $\mathbf{G}$ is a Brillouin zone center and $\mathbf{G} = (h, k, l)$.

INS measurements were carried out at the Institut Laue-Langevin (ILL), in Grenoble, France. Polarized INS data were obtained on the CRG-Jülich and CRG-CEA Grenoble cold and thermal neutron three-axis spectrometers (TASs) IN12 [31] and IN22, respectively. Both TASs were set up in a W configuration and inelastic scans were performed with constant k_f (1.8 Å^{-1} for IN12 and 2.662 Å^{-1} for IN22), where $\mathbf{k}_f$ is the wave vector of the scattered neutron beam.

On IN12, the incident neutron beam spin state was prepared using a transmission polarizing cavity located after the velocity selector and the initial wave vector was selected by a double focusing pyrolytic graphite [PG(002)] monochromator. For IN22, the spin of the incident neutrons was polarized with a vertically focusing Heusler [Cu_2MnAl(111)] monochromator. For both TASs, the neutron polarization and k_f were analyzed using a horizontally focusing Heusler analyzer. All along the neutron path, guide fields were installed to maintain the polarization of the beam. High-order harmonics were suppressed using a velocity selector before the monochromator for IN12 and a PG filter in the scattered neutron beam for IN22. A flipping ratio R of about 22 and 14 has been measured on a graphite sample on IN12 and IN22, respectively. In order to perform longitudinal polarization analysis (LPA), we used a Helmholtz coil setup to control the direction of the polarization on the sample. This method is restricted to temperatures above T_C since the beam gets depolarized when entering the ferromagnetic phase (see the inset of Fig. 5 in Ref. [18] for the temperature dependence of the beam polarization). For investigating the spin dynamics above T_C, the $MnFe_4Si_3$ single crystal was placed inside a cryofurnace.

As a general rule, neutron scattering is only sensitive to magnetic excitations perpendicular to $\mathbf{Q}$ [32] and, by employing LPA, it is possible to separate magnetic fluctuations polarized along different directions in spin space [33]. We use the standard (x, y, z) frame where the x axis is parallel to $\mathbf{Q}$, the z axis is vertical, and the y axis is perpendicular to $\mathbf{Q}$ and z. The corresponding measurement channels where we collected data are canonically labeled NSF$_{xx}$, NSF$_{yy}$, and NSF$_{zz}$, where NSF stands for "non-spin-flip." The neutron scattering double differential cross sections for the three NSF channels are [33]

$$\mathrm{NSF}_{xx} = \left(\frac{d^2\sigma}{d\Omega d\mathrm{E}}\right)^{x}_{\mathrm{NSF}} \propto \mathrm{BG}_{\mathrm{NSF}} + \langle N\rangle, \tag{1}$$

$$\mathrm{NSF}_{yy} = \left(\frac{d^2\sigma}{d\Omega d\mathrm{E}}\right)^{y}_{\mathrm{NSF}} \propto \mathrm{BG}_{\mathrm{NSF}} + \langle N\rangle + \langle \delta M_y\rangle, \tag{2}$$

$$\mathrm{NSF}_{zz} = \left(\frac{d^2\sigma}{d\Omega d\mathrm{E}}\right)^{z}_{\mathrm{NSF}} \propto \mathrm{BG}_{\mathrm{NSF}} + \langle N\rangle + \langle \delta M_z\rangle, \tag{3}$$

where $\mathrm{BG}_{\mathrm{NSF}}$ is the background, $\langle N\rangle$ is the nuclear scattering, and $\langle \delta M_i\rangle$ (with $i = y, z$) are the magnetic fluctuations.

Considering that the scattering plane in our case is (a^*, c), then, for $\mathbf{Q}$ parallel to the $(h00)$ direction, the scattering cross sections are

$$\mathrm{NSF}_{xx} \propto \mathrm{BG}_{\mathrm{NSF}} + \langle N\rangle, \tag{4}$$

$$\mathrm{NSF}_{yy} \propto \mathrm{BG}_{\mathrm{NSF}} + \langle N\rangle + \langle \delta M_c\rangle, \tag{5}$$

$$\mathrm{NSF}_{zz} \propto \mathrm{BG}_{\mathrm{NSF}} + \langle N\rangle + \langle \delta M_b\rangle, \tag{6}$$

and for $\mathbf{Q}$ parallel to the $(00l)$ direction, the scattering cross sections are

$$\mathrm{NSF}_{xx} \propto \mathrm{BG}_{\mathrm{NSF}} + \langle N\rangle, \tag{7}$$

$$\mathrm{NSF}_{yy} \propto \mathrm{BG}_{\mathrm{NSF}} + \langle N\rangle + \langle \delta M_{a^*}\rangle, \tag{8}$$

$$\mathrm{NSF}_{zz} \propto \mathrm{BG}_{\mathrm{NSF}} + \langle N\rangle + \langle \delta M_b\rangle. \tag{9}$$

Therefore, one can extract the magnetic fluctuations polarized along different directions by canonical subtraction of intensities in different NSF channels. Similar analysis can be performed in the "spin-flip" (SF) channel. A few data (not shown) were collected in the SF channel. The subtracted spectra in SF were found to be identical to the ones obtained in the NSF channel; therefore, the latter channel was chosen for the full data collection. Finally, given the obtained flipping ratios ($R > 13$) and the limited statistics of the data, polarization corrections (of the order of $1/R$) were not performed.

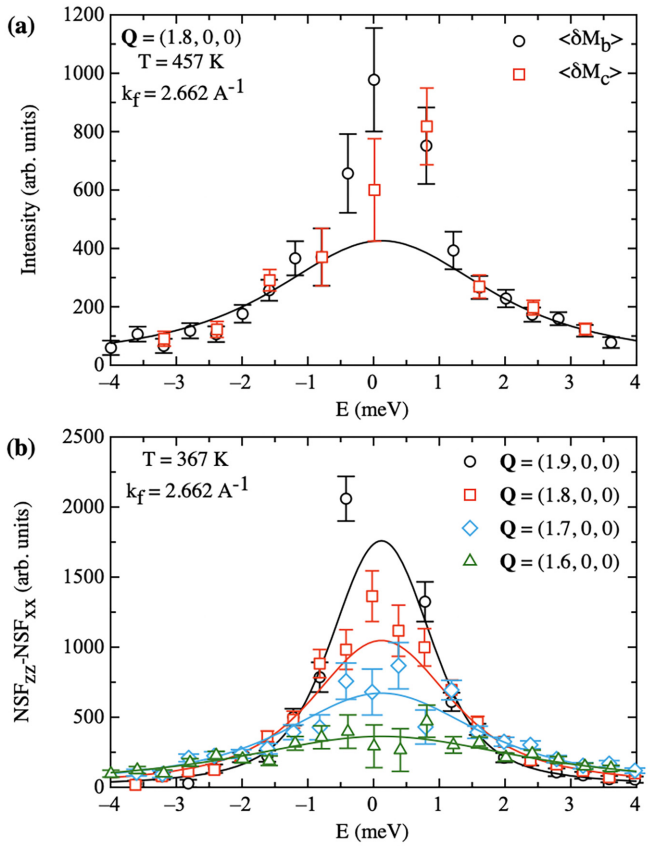

FIG. 1. (a) $\langle \delta M_b \rangle$ and $\langle \delta M_c \rangle$ spin fluctuations spectra of $MnFe_4Si_3$ from constant **Q** scans at $\mathbf{Q} = (1.8, 0, 0)$ at $T = 457$ K. (b) $\langle \delta M_b \rangle$ spin fluctuations spectra obtained at different Q_h positions along the $(h00)$ direction at $T = 367$ K. Solid lines represent fits, as explained in the text.

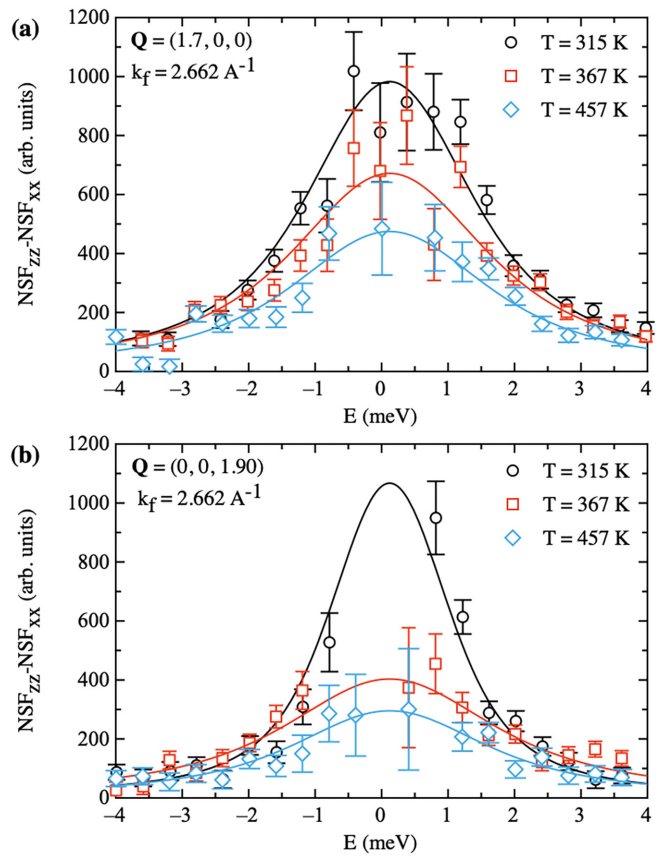

FIG. 2. $\langle \delta M_b \rangle$ spin fluctuations spectra of $MnFe_4Si_3$ obtained at different temperatures and measured at (a) $\mathbf{Q} = (1.7, 0, 0)$ and (b) $\mathbf{Q} = (0, 0, 1.9)$. Solid lines represent fits, as explained in the text.

In addition, unpolarized INS data under magnetic field were obtained at IN12 with $k_f = 1.8$ $Å^{-1}$. The PG(002) monochromator was vertically focused and a horizontally focused PG(002) analyzer was used, and 40′-open-open collimations were installed. The $MnFe_4Si_3$ single crystal was placed inside a 2.5 T vertical field magnet. The magnetic field was applied parallel to the b axis of the hexagonal system of the sample [perpendicular to the (a^*, c) plane].

III. EXPERIMENTAL RESULTS

A. Temperature dependence of paramagnetic scattering without magnetic field

To investigate the spin dynamics of $MnFe_4Si_3$ above the Curie temperature, spectra were collected at different temperatures, namely, 315, 336, 367, 396, 427, and 457 K, which is about $1.033 \times T_C$, $1.1 \times T_C$, $1.2 \times T_C$, $1.3 \times T_C$, $1.4 \times T_C$, and $1.5 \times T_C$, respectively. Constant **Q** scans were carried out at energy transfers $-4 \leqslant E \leqslant 4$ meV around the Brillouin zone centers $\mathbf{G} = (2, 0, 0)$ and $\mathbf{G} = (0, 0, 2)$ and data were obtained along the $(h00)$ and $(00l)$ directions.

Figure 1(a) shows the in-plane $\langle \delta M_b \rangle$ and out-of-plane $\langle \delta M_c \rangle$ fluctuations spectra at $\mathbf{Q} = (1.8, 0, 0)$ in the maximum investigated temperature of $1.5 \times T_C$. $\langle \delta M_b \rangle$ and $\langle \delta M_c \rangle$ were obtained by making the subtractions Eq. (6)−Eq. (4) and Eq. (5)−Eq. (4), respectively. We observe broad energy distributions centered at zero-energy transfer (quasielastic excitations) that mark the existence of diffusive modes and are typical features of paramagnetic scattering [1]. Moreover, as can be seen at this temperature, $\langle \delta M_b \rangle$ and $\langle \delta M_c \rangle$ are found to be identical, pointing to isotropic fluctuations (Heisenberg spins). In a previous study [18], similar behavior was established for $1.036 \times T_C$ and, therefore, one can assume that the dynamical spin susceptibility will remain isotropic in all of the intermediate-temperature range of $315 \leqslant T \leqslant 457$ K. Figure 1(b) depicts the subtracted energy spectra between two NSF channels (NSF_{zz} and NSF_{xx}) acquired along the $(h00)$ direction at $1.2 \times T_C$. As expected, with increasing q, the intensity decreases while the signal broadens. The spin fluctuations do not only change significantly with q, but are also strongly temperature dependent, as illustrated in Fig. 2. For a given scattering vector, one observes a substantial diminution of the spectral weight with increasing temperature, which is more prominent along the $(00l)$ direction. Following the evidence for isotropy in spin space, the data were collected only for $\langle \delta M_b \rangle$ and the outcome is described in the next section.

In order to analyze the obtained spectra, we followed the same procedure which is given in detail in Ref. [18]. Briefly we mention that the subtracted intensities were convoluted with the one-dimensional (1D)-instrument resolution in the energy direction, and the PM scattering for the energy transfer

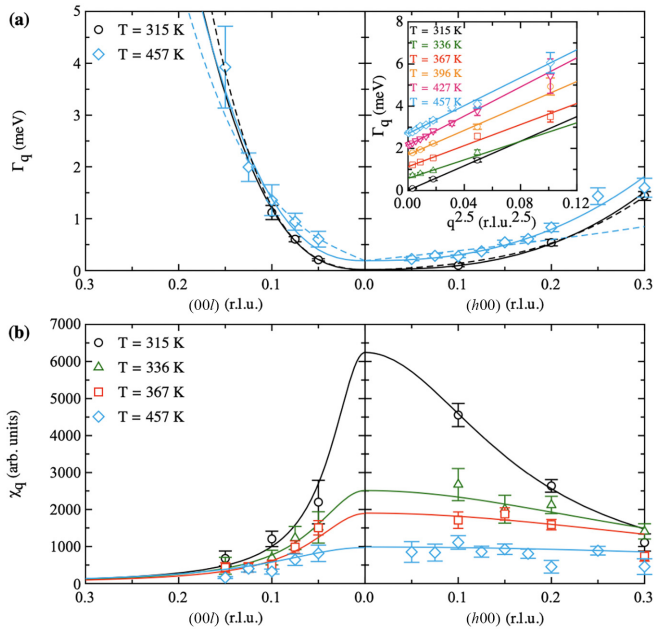

FIG. 3. (a) Linewidths Γ_q and (b) q-dependent susceptibility χ_q of $MnFe_4Si_3$ obtained along the $(00l)$ and $(h00)$ directions at different temperatures. For clarity, only the results of Γ_q obtained at the minimum and maximum investigated temperature are shown. The solid and dashed lines for Γ_q correspond to fits with the models of Heisenberg and weak itinerant ferromagnetism, respectively, while for χ_q, solid lines indicate fits with Lorentzian functions. The inset in (a) shows the linear behavior for $\Gamma_q(T)$ vs $q^{2.5}$ for the $(h00)$ direction. For clarity, the data (in the inset only) are shifted by a constant value along the vertical axis.

in the range $-4 \leqslant E \leqslant 4$ meV can be described with the empirical double Lorentzian function [11],

$$S(\mathbf{Q}, E) = k_B T \frac{\chi_0}{1 + (q/\kappa)^2} \frac{\Gamma_q}{E^2 + \Gamma_q^2} = k_B T \frac{\chi_q \Gamma_q}{E^2 + \Gamma_q^2}, \quad (10)$$

where χ_0, κ, Γ_q, and χ_q are the static susceptibility, the inverse spin correlation length, the q-dependent energy linewidth (relaxation rate), and the q-dependent susceptibility, respectively. The obtained values for Γ_q and χ_q for the $(00l)$ and $(h00)$ directions at different temperatures are shown in Fig. 3.

The q-dependent energy linewidth between the $(00l)$ and $(h00)$ high-symmetry directions of the hexagonal system is strongly anisotropic [see Fig. 3(a)], in line with the results obtained for the spin-wave spectrum measured below T_C [18]. To describe the experimental data at $T = 1.5 \times T_C = 457$ K, we use two different models [11]: the expression for weak itinerant FM, $\Gamma_q = \Gamma_0 + A_{\rm wi} q[1 + (q/\kappa)^2]$, and the empirical formula, $\Gamma_q = \Gamma_0 + Aq^z$, where Γ_0 refers to the $q = 0$ intercept of Γ_q. The data are better described by the latter formula and we obtain a finite value for Γ_0 and the exponent $z = 2.44(19)$. The exponent is close to $z = 2.5$, which describes the relaxation rate of the magnetic fluctuations for Heisenberg ferromagnets [11]. In a previous study [18], the experimental data for the relaxation rates at $T = 1.036 \times T_C = 316$ K could be well described by both models, i.e., the model for a Heisenberg FM as well as the model for a weak itinerant FM. However, in the present work, we demonstrate that at $T = 1.5 \times T_C$, only the former model is suitable for Γ_q [see solid lines in Fig. 3(a)]. Consequently, the model $\Gamma_q(T) = \Gamma_0(T) + A(T)q^{2.5}$ was used to fit the data in the present work for $T \leqslant 457$ K. A zoom of the low-q data obtained along $(h00)$ is shown in the inset of Fig. 3(a), where Γ_q is plotted as a function of $q^{2.5}$.

Figure 3(b) shows the temperature dependence of the q-dependent susceptibility χ_q. For all the investigated temperatures, χ_q decreases faster along the $(00l)$ direction compared to $(h00)$, indicating a shorter inverse correlation length. We used a Lorentzian function for χ_q, $\chi_q^{-1} = \chi_0^{-1}[1 + (q/\kappa)^2]$ [see Eq. (10)], in order to extract the values for the static susceptibility χ_0 and the inverse correlation lengths κ. All of the experimentally obtained results of Γ_0, A, χ_0, and κ for each temperature are summarized in Table I. While A substantially depends on direction in line with Γ_q, it is weakly affected by temperature. All other quantities in Table I change significantly with temperature. The $q = 0$ susceptibility χ_0 strongly decreases with increasing temperature, pointing to the criticality of spin fluctuations near T_C. However, its precise temperature dependence (not shown) does not follow a $1/T$-like behavior in relation to the fact that the Curie-Weiss law was found to describe the bulk susceptibility data only for $T > 550$ K [29]. Γ_0 follows an inverse temperature variation compared to χ_0. Following the behavior of χ_q, the inverse spin correlation lengths κ are strongly temperature and directional dependent. The quantities κ, A, and Γ_0 that quantify the extent of spin fluctuation in $(\mathbf{q}, E)$ space are viewed in detail in Sec. IV.

B. Field dependence of paramagnetic scattering at $1.036 \times T_C$

In a previous study, it was shown that a magnetic field of 2 T suppresses the elastic contribution measured at low

TABLE I. Microscopic parameters describing the spin fluctuation spectrum of ferromagnetic $MnFe_4Si_3$ at different temperatures in the paramagnetic state. Data were not measured for the $(00l)$ direction at $T = 427$ K.

T (K)	Γ_0 (meV)	$A_{(h00)}$ (meVÅ$^{2.5}$)	$A_{(00l)}$ (meVÅ$^{2.5}$)	χ_0 (arb. units)	$\kappa_{(h00)}$ (Å^{-1})	$\kappa_{(00l)}$ (Å^{-1})
315	0.002(5)	24.8(6)	184(6)	6200(1100)	0.161(23)	0.054(13)
336	0.050(21)	20(3)	155(18)	2500(500)	0.388(108)	0.088(19)
367	0.087(17)	24(3)	179(14)	1720(190)	0.490(104)	0.104(16)
396	0.119(25)	28(2)	164(17)	1400(140)	0.55(13)	0.117(27)
427	0.135(22)	31(2)		1040(150)	0.800(211)	
457	0.190(29)	32(3)	153(19)	987(111)	0.807(223)	0.16(4)

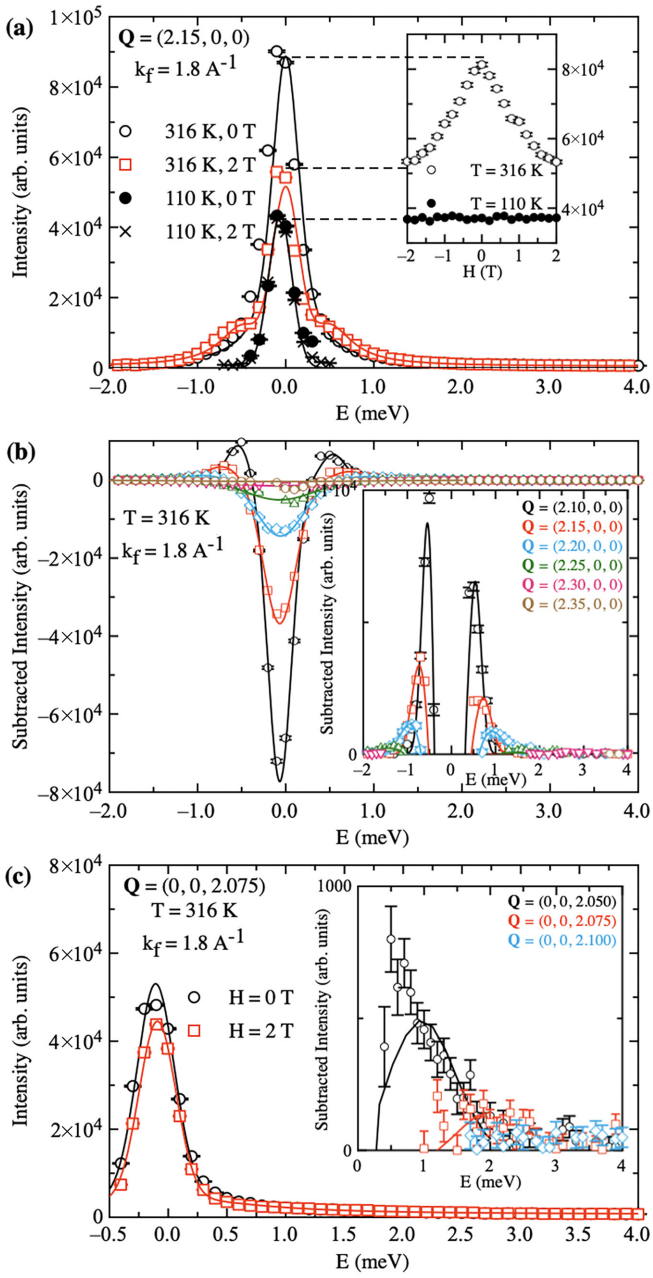

FIG. 4. Spin fluctuations spectra of $MnFe_4Si_3$ obtained at $H = 0$ T and $H = 2$ T and measured at (a) $\mathbf{Q} = (2.15, 0, 0)$ and (c) $\mathbf{Q} = (0, 0, 2.075)$. (a) The signal obtained at 110 K at 0 and 2 T for $\mathbf{Q} = (2.15, 0, 0)$ indicates the incoherent background. The inset shows the field dependence of $\mathbf{Q} = (2.15, 0, 0)$ at zero-energy transfer at 316 and 110 K. (b) Subtracted intensities $[I(2\,\mathrm{T}) - I(0\,\mathrm{T})]$ at $T = 316$ K at different $\mathbf{Q}$ positions along the $(h00)$ direction. The insets in (b) and (c) focus on the positive part of the subtracted intensities $[I(2\,\mathrm{T}) - I(0\,\mathrm{T})]$ at $T = 316$ K for the $(h00)$ and $(00l)$ directions, respectively. Lines are guides for the eyes.

Q close to T_C and integrated in the energy range -0.1 to 0.1 meV (see Fig. 6 in Ref. [18]). A similar measurement is shown for a higher-Q position in the inset of Fig. 4(a) through a field dependence of the intensity for $\mathbf{Q} = (2.15, 0, 0)$ for zero-energy transfer at 316 and 110 K (with the experimental configuration presented above). The intensity at 316 K decreases with magnetic field, while the measurement at 110 K is field independent and corresponds to the incoherent background (note that this contribution is canceled by subtraction in the polarized data shown in the previous section). At $|H| = 2$ T, the remaining magnetic signal is above this background; however, a considerable amount ($\approx 2/3$) of magnetic elastic signal is suppressed. The amount of suppression is found to be $\mathbf{q}$ dependent.

In order to further understand the field evolution of the magnetic excitation spectrum, the energy dependence of the fluctuations was comparatively studied at zero and finite magnetic field up to an energy transfer of 4 meV. Spectra along the $(h00)$ and $(00l)$ directions were collected at 316 K at $H = 0$ and $H = 2$ T. Representative measurements are shown in Figs. 4(a) and 4(c) for $\mathbf{Q} = (2.15, 0, 0)$ and $\mathbf{Q} = (0, 0, 2.075)$, respectively. Consistently with the polarized data (see Figs. 1 and 2), a signal centered at $E = 0$ meV is observed for both directions at 0 T. Applying a magnetic field of 2 T results in a reduction of this PM scattering consistent with the field scan presented in the inset of Fig. 4(a), as indicated by the dashed lines [for $\mathbf{Q} = (2.15, 0, 0)$, the incoherent background signal obtained at 110 K for 0 T and 2 T is also shown]. The $\mathbf{Q}$ dependence of the subtracted intensities, $I(2\,\mathrm{T}) - I(0\,\mathrm{T})$, is shown in Fig. 4(b) for the $(h00)$ direction. In the quasielastic regime (low-energy transfers), it is negative and decreases in absolute value when q increases. At higher energies and small wave vectors, this difference is positive and the spectra show a local maximum at finite-energy transfers which position disperses with respect to the wave vector. This is better highlighted in the insets of Figs. 4(b) and 4(c) for the $(h00)$ and $(00l)$ directions, respectively. This peak at finite energy corresponds to spin waves associated with the fact that the paramagnetic system reenters the ferromagnetic phase under finite magnetic field. Such phenomena are rarely reported in neutron scattering studies, with examples being the FM Gd [34] and EuS [35].

IV. DISCUSSION

A. Nature of spin fluctuations

First, by analyzing the results for κ, we acquire information of the typical length scales of the system. For the inverse of the spin correlation lengths, one can assume that they follow the critical law $\kappa = \kappa_0 \tau^{\nu}$ [11], where $\tau = (T/T_C - 1)$ is the reduced temperature. Such a fit yields $\kappa_0^{(h00)} = 1.25(24)$ Å^{-1}, $\kappa_0^{(00l)} = 0.24(2)$ Å^{-1}, and $\nu = 0.56(8)$ [see Fig. 5(b)]. The obtained values for κ_0 are close to the ones previously extracted from the spin-wave stiffness D, using the relation $\kappa_0^2 = 3k_B T_C/(S+1)D$ [18,36], while ν approaches the value of 0.5 which corresponds to the exponent in the mean-field approximation. For $MnFe_4Si_3$ when considering the lattice parameters [29], it becomes evident that the interatomic distances are comparable to κ_0^{-1}, which points to a localized magnetic system.

Second, we analyze the results for the relaxation rates in view of extracting the characteristic energy scales. As discussed in Sec. III, the data can be well described in the whole investigated temperature range by the formula $\Gamma_q(T) = \Gamma_0(T) + A_q(T)q^{2.5}$. It is found that the $q = 0$ relaxation rate, $\Gamma_0(T)$, increases linearly with temperature and vanishes at T_C,

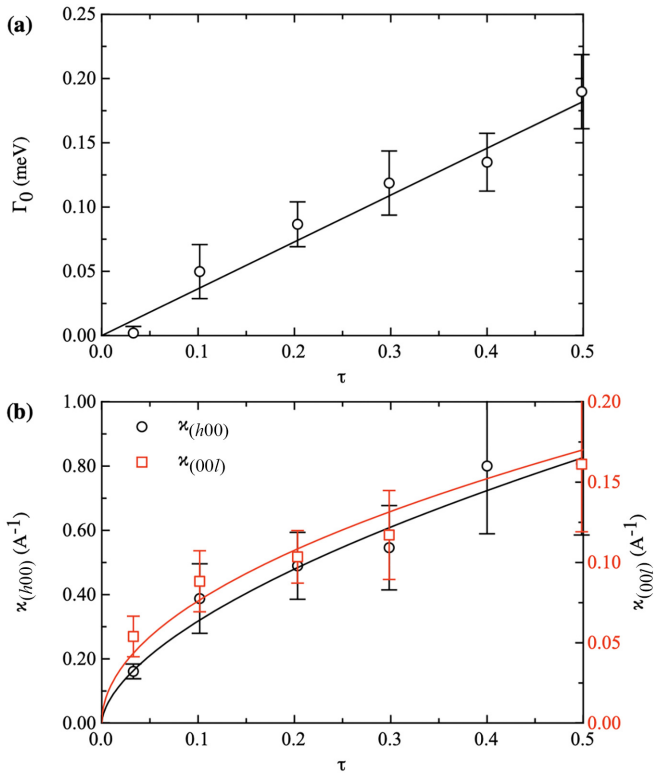

FIG. 5. Temperature dependence of (a) Γ_0 and (b) the inverse spin correlation lengths κ along $(h00)$ (left axis scale) and $(00l)$ (right axis scale) of $MnFe_4Si_3$. τ is the reduced temperature. Solid lines represent fits, as explained in the text.

following $\Gamma_0(\tau) = 0.36(3)\tau$ [see Fig. 5(a)]. Given the relation between κ and τ, we consequently obtain $\Gamma_0 \propto \kappa^2$. This specific law is the signature of pseudodipolar interactions (interplay between crystal-field and spin-orbit interactions) being responsible for the finite relaxation rate at $q = 0$ [37,38]. When Γ_q is finite at $q = 0$, the spin dynamics is called "nonconserved" since the conservation of magnetization (i.e., the magnetization commutes with the Hamiltonian), which implies that $\Gamma_{q=0} = 0$, is necessarily broken. The coefficient A is weakly temperature dependent, which makes it a pertinent parameter to quantify the spread of spin fluctuations in E space. Since the exponents linking Γ_0 with κ, and Γ_q with q, are different, the data cannot collapse on a single scaling function of the form $\Gamma_q(T) = Aq^z f(\kappa/q)$, with all the T dependence being included in κ. It is recalled that when such scaling is valid, f follows a nonmonotonic Résibois-Piette function [39] for the Heisenberg model, while in itinerant magnets, f is monotonic with $f(\kappa/q) = [1 + (\kappa/q)^2]$ [11]. At T_C, where $\kappa = 0$, $\Gamma_q = Aq^z$ with $z = 2.5$ for Heisenberg systems and $z = 3$ for itinerant magnets [1,11]. The behavior at T_C is persistent even in the absence of scaling since $\Gamma_0(T_C) = 0$. It was found experimentally that the exponent $z = 2.5$ works fairly well even for the archetypal itinerant magnet Ni_3Al [9] and, to a lesser extent, for MnSi [4] (note that MnSi is not a ferromagnet, but a helimagnet with a very long period). Therefore, a quantitative comparison of the spin fluctuations of different isotropic ferromagnets can be made using an exponent $z = 2.5$ to describe the q dependence of the relaxation rate near T_C.

To compare the results of this study for $MnFe_4Si_3$ with the existing data for various isotropic cubic ferromagnets, we adopt the approach of Ref. [54]. From the results gathered in the literature, we calculate the characteristic energies of each FM at the Brillouin zone boundary $\Gamma_{ZB}(T_C) = Aq_{ZB}^{2.5}$ [for $MnFe_4Si_3$, the given values are $\Gamma_{ZB}(315\ K)$]. The results are summarized in Table II and the lines are arranged by decreasing Γ_{ZB}/k_BT_C, i.e., from more itinerant to more localized systems. It is known that for localized Heisenberg insulators (EuO and EuS), $\Gamma_{ZB} \approx k_BT_C$, while for metallic itinerant magnets, $\Gamma_{ZB} \gg k_BT_C$ [11]. From Table II, one concludes that $MnFe_4Si_3$ can be categorized as a localized FM system. It should be noted that the $q^{2.5}$ dependence of the relaxation rate is surprisingly found to be valid in the wave-vector range $\kappa \sim q$ for $(h00)$ and $(00l)$, as well as in $\kappa \gg q$ for $(h00)$, while it is expected to hold in the critical regime $q \gg \kappa$. This latter regime cannot be reached in our experiment for different reasons, depending on the direction that is probed: along $(h00)$, high values of κ are obtained already at 315 K, and along $(00l)$, the intensity drops too fast as a function of q. The hydrodynamic regime, corresponding to $\Gamma_q \propto q^2$ and expected for $\kappa \gg q$, is hidden by the residual relaxation rate $\Gamma_0 \propto \kappa^2$ due to the large κ [38]. To summarize this section, the extension of spin fluctuations both in $\mathbf{q}$ and E space, quantified by κ_0 and A, respectively, points towards localized magnetism for $MnFe_4Si_3$.

B. Comparison with other magnetocaloric compounds

Within intermetallic compounds containing Mn and/or Fe, $(Mn, Fe)_2(P,Si)$ and $LaFe_{13-x}Si_x$ stand out for their remarkable MCE characteristics [15]. Both systems are considered as itinerant magnetic compounds, although in $(Mn, Fe)_2(P,Si)$, a scenario sometimes put forward is the one of mixed magnetism, where local and itinerant moments coexist [55]. Sizeable spin fluctuations were evidenced by INS for both $(Mn, Fe)_2(P,Si)$ [20] and $LaFe_{13-x}Si_x$ [21–23]. These studies did not take the canonical approach followed in the present work and hence did not provide microscopic parameters such as the bare inverse spin correlation length κ_0 or the A coefficient of the power law linking the relaxation rate to the wave vector. In contrast to these itinerant magnets, we have shown by INS that the $MnFe_4Si_3$ system is clearly characterized by local magnetism above room temperature, despite the occurrence of several magnetic sites that could favor mixed magnetism (WP 4d nonmagnetic site with Fe occupancy and WP 6g magnetic site with mixed Fe/Mn occupancy [29]). It would be interesting to investigate the paramagnetic fluctuations in other promising FM compounds containing Fe or Mn, which could be developed for magnetic refrigeration applications, and spin dynamics investigations below T_C have already been carried out, e.g., Fe_2P [56], Mn_5Ge_3 [57], MnBi [58], MnSb [59,60], and MnP [61], in order to reveal their nature of magnetism.

C. Spin fluctuations and magnetocaloric effect

The magnetic excitation spectrum measured by neutron scattering above T_C reflects the importance of thermal fluctuations to which the entropy is also related. A quantitative

TABLE II. Microscopic parameters describing the spin fluctuations for various ferromagnets. Γ_{ZB} is the relaxation rate at the Brillouin zone boundary in the [111] direction for Ni, CoS_2, Co, Pd_2MnSn, EuO, and EuS, and in [110] for Ni_3Al, MnSi, and α-Fe. κ_0^+ refers to the inverse spin correlation length determined from measurements above T_C (different values of ν are reported between the mean field $\nu = 0.5$ and the Heisenberg critical value $\nu = 0.7$ depending on the systems and the temperature range that are studied). For a given material, the parameters reported in the literature can be spread out due to different experimental conditions or different data analysis methods, and the references of the mentioned study are given for each value of the table. $\Delta T_{ad}/H$ is the estimated rate of change of the adiabatic temperature per Tesla at T_C using the relevant references (see Appendix A). The results for $MnFe_4Si_3$ are obtained from this work and values are given for the [100] and [001] directions. The A_0 values for $MnFe_4Si_3$ are given at 315 K. The blank spaces in the table indicate unreported values to our knowledge. The lines of the table for the cubic ferromagnets are sorted by decreasing Γ_{ZB}/k_BT_C.

		k_BT_C	A_0	Γ_{ZB}	Γ_{ZB}/k_BT_C	κ_0^+	Lattice constant	$\Delta T_{ad}/H$
Material	Space group	(meV)	(meVÅ$^{2.5}$)	(meV)		(Å^{-1})	(Å)	(K/T)
Ni_3Al	$Pm\bar{3}m$	6.3	226(7) [40]	390	61.9	0.049(19) [9]	3.57	
Ni	$Fm\bar{3}m$	54.6	367(18) [41]	1075	19.7	0.81(4) [42]	3.54	0.68 [17]
CoS_2	$Pa\bar{3}$	10.4	86(2) [8]	82.9	7.97	0.232 [8]	5.52	1.2 [43,44]
MnSi	$P2_13$	2.6	19.6 [4]	18.4	7.08	0.18 [4]	4.56	1.3 [45]
Co	$Fm\bar{3}m$	119.5	300(30) [46]	837	7.01	0.98(4) [47]	3.61	1.4 [17]
α-Fe	$Im\bar{3}m$	89.8	135(5) [48]	402	4.48	0.82(3) [49]	2.87	2.1 [17]
Pd_2MnSn	$Fm\bar{3}m$	16.4	60 [5]	40.3	2.46	0.22 [5]	6.38	
EuO	$Fm\bar{3}m$	5.9	8.3(7) [50]	9.57	1.62	0.64(4) [50]	5.14	1.6 [51]
EuS	$Fm\bar{3}m$	1.4	2.1(3) [6]	1.73	1.24	0.55(3) [47]	5.88	2.9 [52]
$MnFe_4Si_3$	$P6_3/mcm$	26.3	24.8(6)	5.14	0.20	1.25(24)	6.81 (a axis)	0.59 [53]
			184(6)	66.2	2.52	0.24(2)	4.73 (c axis)	

connection can be achieved between the magnetic entropy and the spin fluctuation spectrum in the limit $T \to 0$ K [62,63], which is very useful to relate the spin dynamics with the Sommerfeld coefficient obtained from specific heat measurements as demonstrated in correlated electron systems [64–66]. However, such common approximation is not valid at high temperatures due to interactions between individual spin fluctuations. In Appendix B, we develop an alternate approach to relate the entropy $\mathcal{S}$ to the scattering function $S_i(\mathbf{Q}, E)$ based on the neutron sum rule. The obtained magnetic field derivative of the entropy $\mathcal{S}$ is

$$\left(\frac{\partial \mathcal{S}}{\partial H}\right)_T = -\frac{1}{2MV^2}\frac{\partial}{\partial T}\sum_{i,\mathbf{Q}}\int_{-\infty}^{\infty} S_i(\mathbf{Q}, E)dE, \qquad (11)$$

where i=($\parallel$, $\perp$) corresponds to the response parallel or perpendicular to the applied magnetic field. This distinction arises because the magnetic field necessarily breaks the isotropy of spin fluctuations [67]. In Fig. 4, the data obtained at 2 T are the sum of these contributions and a difficulty originates from the fact that they may have different characteristic linewidths with different temperature variations. This separation would be an enormous experimental task in terms of neutron beam time; basically, the $H = 0$ T approach presented above should be repeated with polarized neutrons under field, for the two channels $i = (\parallel, \perp)$.

In addition, as shown in Sec. III, two effects occur under field: (i) the low-energy diffuse scattering (quasielastic signal) is suppressed at 2 T and (ii) spin waves are induced at higher energy. Analyzing all these aspects in a quantitative way with the limited set of available data is beyond the scope of this paper. Equation (11) indicates that the strong modification of the excitation spectrum under magnetic field is correlated with the change of magnetic entropy of the system and the magnetocaloric effect. Staying on qualitative grounds, our data show that the quasielastic signal is strongly affected by a field of 2 T and that the field-induced excitations are constituted of a dispersive mode. It can be safely inferred that a higher field will suppress all quasielastic signals to the benefit of the field-induced spin-wave mode (and the field-induced order parameter). Globally, this should translate into a decrease of the magnetic entropy of the system under magnetic field, as experimentally reported in single crystals of $MnFe_4Si_3$ with an entropy change of about -2 J/kgK at a field change from 0 to 2 T along the [100] direction at 316 K [29].

V. CONCLUSIONS

By a detailed INS study of the spin fluctuation spectrum of $MnFe_4Si_3$, we have shown that the nature of the magnetism of this material is localized above room temperature. This conclusion stems from the characteristic extent in both wave-vector and energy space of the fluctuation spectrum. In the studied temperature range, $315 \leqslant T \leqslant 457$ K, the inverse correlation lengths κ follow a temperature dependence close to the mean-field behavior (exponent $\nu = 0.5$), and the bare inverse correlation lengths κ_0 are comparable to the interatomic distances. The relaxation rate follows $\Gamma_q(T) = \Gamma_0(T) + A(T)q^{2.5}$ in an extended $\mathbf{q}$ range, where the $z = 2.5$ exponent is characteristic of Heisenberg ferromagnets. The $q = 0$ intercept Γ_0 vanishes at T_C and follows $\Gamma_0 \propto \kappa^2$, which indicates that pseudodipolar interactions are responsible for the nonconserved spin dynamics. The magnetic field response evidences a suppression of the quasielastic signal at 2 T and the appearance of a magnetic field-induced spin-wave mode at finite energy. This strong modification of the fluctuation spectrum is associated with the reduction of the system's entropy under magnetic field. While a quantitative analysis cannot be

achieved in the present study, a route to link magnetic entropy and spin fluctuations is proposed for further experimental investigations which could be combined with theoretical modeling. Undertaking canonical spin fluctuation studies in more magnetic systems will provide important information about microscopic magnetic properties, which in turn could help define strategies for improving specific materials for magnetic refrigeration applications.

ACKNOWLEDGMENTS

N.B. acknowledges the support of JCNS through the Tasso Springer Fellowship and the Czech Science Foundation GAČR under the Junior Star Grant No. GM21-24965M (MaMBA).

DATA AVAILABILITY

The neutron data collected at the ILL are available at Refs. [68–70].

APPENDIX A: ADIABATIC TEMPERATURE CHANGE OF TABLE II

For completeness, the adiabatic temperature change $\Delta T_{\rm ad}$ corresponding to the materials temperature variation for an adiabatic magnetic field change ΔH is given for the different compounds listed in Table II. The available measurements of $\Delta T_{\rm ad}$ are obtained with different ΔH and we estimate the rate of change of $\Delta T_{\rm ad}$ per Tesla. This allows a comparison between the different systems; however, it should be noted that $\Delta T_{\rm ad} \not\propto \Delta H$, but generally decreases as the applied magnetic field increases [17]. When considering the infinitesimal adiabatic temperature change,

$$dT(T,H) = -\left(\frac{T}{C(T,H)}\right)_H \left(\frac{\partial M(T,H)}{\partial T}\right)_H dH, \quad \text{(A1)}$$

where M is the magnetization and C the specific heat at constant pressure, it is obvious that the Curie temperature (or, equivalently, the operating temperature near T_C) and the specific heat will be determinant (and counterbalancing) factors. Given the fact that the factors entering in Eq. (A1) are highly materials dependent, it is not pertinent to extract a trend between microscopic magnetism and MCE over the variety of compounds listed in Table II. Indeed, MCE properties are usually reviewed on experimental grounds considering the materials or the different families of materials one by one [15–17].

APPENDIX B: MAGNETIC NEUTRON SCATTERING SUM RULE, FLUCTUATIONS, AND ENTROPY

The isothermal entropy change $\Delta\mathcal{S}$ can be obtained through an integration of the infinitesimal change,

$$d\mathcal{S}(T,H) = \left(\frac{\partial \mathcal{S}(T,H)}{\partial H}\right)_T dH, \quad \text{(B1)}$$

which is often evaluated from the magnetization measurements using the Maxwell's relation,

$$\left(\frac{\partial \mathcal{S}(T,H)}{\partial H}\right)_T = \left(\frac{\partial M(T,H)}{\partial T}\right)_H. \quad \text{(B2)}$$

For a localized magnetic system, the neutron sum rule is

$$s(s+1) = \langle m\rangle^2 + \sum_{i,\mathbf{Q}} \int_{-\infty}^{\infty} S_i(\mathbf{Q},E)dE, \quad \text{(B3)}$$

where s is the effective spin of the ground state and $\langle m\rangle$ is the ferromagnetic moment per site ($M{=}\langle m\rangle/V$, with V the volume of the unit cell). The derivative of Eq. (B3) gives an alternate way to estimate the change of entropy with field,

$$\begin{aligned} 2MV^2\left(\frac{\partial M}{\partial T}\right)_H &= 2MV^2\left(\frac{\partial \mathcal{S}}{\partial H}\right)_T \\ &= -\frac{\partial}{\partial T}\sum_{i,\mathbf{Q}} \int_{-\infty}^{\infty} S_i(\mathbf{Q},E)dE. \end{aligned} \quad \text{(B4)}$$

This relation between magnetization, entropy, and spin fluctuations is only valid for local magnetism since it derives from the sum rule in Eq. (B3). Interestingly, it shows that the change of entropy with field is related to the ratio of the temperature derivative of the wave-vector and energy integrated scattering function to the magnetization and, hence, it clearly shows the role of spin fluctuations that is implicit in Eq. (B2). It is indeed explicit from Eq. (B4) that the temperature derivative of the magnetization is controlled by the magnetic excitation spectrum.

[1] T. Moriya, *Spin Fluctuations in Itinerant Electron Magnetism* (Springer-Verlag, Berlin, 1985).
[2] J. P. Wicksted, P. Böni, and G. Shirane, Polarized-beam study of the paramagnetic scattering from bcc iron, Phys. Rev. B **30**, 3655 (1984).
[3] O. Steinsvoll, C. F. Majkrzak, G. Shirane, and J. Wicksted, Paramagnetic scattering from metallic Ni, Phys. Rev. B **30**, 2377 (1984).
[4] Y. Ishikawa, Y. Noda, Y. J. Uemura, C. F. Majkrzak, and G. Shirane, Paramagnetic spin fluctuations in the weak itinerant-electron ferromagnet MnSi, Phys. Rev. B **31**, 5884 (1985).
[5] M. Kohgi, Y. Endoh, Y. Ishikawa, H. Yoshizawa, and G. Shirane, High-temperature spin dynamics of a cubic ferromagnet Pd_2MnSn, Phys. Rev. B **34**, 1762 (1986).
[6] P. Böni, G. Shirane, H. G. Bohn, and W. Zinn, Critical magnetic scattering from the Heisenberg ferromagnet EuS, J. Appl. Phys. **61**, 3397 (1987).
[7] P. Böni, M. E. Chen, and G. Shirane, Comparison of the critical magnetic scattering from the Heisenberg system EuO with renormalization-group theory, Phys. Rev. B **35**, 8449 (1987).
[8] H. Hiraka, Y. Endoh, and K. Yamada, Dynamical susceptibility in ferromagnetic metal of CoS_2 - Inelastic magnetic neutron scattering, J. Phys. Soc. Jpn. **66**, 818 (1997).
[9] F. Semadeni, B. Roessli, P. Böni, P. Vorderwisch, and T. Chatterji, Critical fluctuations in the weak itinerant ferromagnet Ni_3Al: A comparison between self-consistent renormalization and mode-mode coupling theory, Phys. Rev. B **62**, 1083 (2000).

[10] J. Kindervater, S. Säubert, and P. Böni, Dipolar effects on the critical fluctuations in Fe: Investigation by the neutron spin-echo technique MIEZE, Phys. Rev. B **95**, 014429 (2017).

[11] Y. Endoh and P. Böni, Magnetic excitations in metallic ferro- and antiferromagnets, J. Phys. Soc. Jpn. **75**, 111002 (2006).

[12] S. Raymond, J. Panarin, F. Givord, A. P. Murani, J. X. Boucherle, and P. Lejay, Low-energy magnetic excitation spectrum of the unconventional ferromagnet $CeRh_3B_2$, Phys. Rev. B **82**, 094416 (2010).

[13] C. Stock, D. A. Sokolov, P. Bourges, P. H. Tobash, K. Gofryk, F. Ronning, E. D. Bauer, K. C. Rule, and A. D. Huxley, Anisotropic critical magnetic fluctuations in the ferromagnetic superconductor UCoGe, Phys. Rev. Lett. **107**, 187202 (2011).

[14] F. Haslbeck, S. Säubert, M. Seifert, C. Franz, M. Schulz, A. Heinemann, T. Keller, Pinaki Das, J. D. Thompson, E. D. Bauer, C. Pfleiderer, and M. Janoschek, Ultrahigh-resolution neutron spectroscopy of low-energy spin dynamics in UGe_2, Phys. Rev. B **99**, 014429 (2019).

[15] F. Zhang, X. Miao, N. van Dijk, E. Brück, and Y. Ren, Advanced magnetocaloric materials for energy conversion: Recent progress, opportunities, and perspective, Adv. Energy Mater. **14**, 2400369 (2024).

[16] V. Franco, J.S. Blázquez, B. Ingale, and A. Conde, The magnetocaloric effect and magnetic refrigeration near room temperature: Materials and models, Annu. Rev. Mater. Res. **42**, 305 (2012).

[17] K. A. Gschneidner and V. K. Pecharsky, Magnetocaloric Materials, Annu. Rev. Mater. Sci. **30**, 387 (2000).

[18] N. Biniskos, S. Raymond, K. Schmalzl, A. Schneidewind, J. Voigt, R. Georgii, P. Hering, J. Persson, K. Friese, and T. Brückel, Spin dynamics of the magnetocaloric compound $MnFe_4Si_3$, Phys. Rev. B **96**, 104407 (2017).

[19] N. Biniskos, K. Schmalzl, S. Raymond, S. Petit, P. Steffens, J. Persson, and T. Brückel, Spin fluctuations drive the inverse magnetocaloric effect in Mn_5Si_3, Phys. Rev. Lett. **120**, 257205 (2018).

[20] X. F. Miao, L. Caron, J. Cedervall, P. C. M. Gubbens, P. Dalmas de Réotier, A. Yaouanc, F. Qian, A. R. Wildes, H. Luetkens, A. Amato, N. H. van Dijk, and E. Brück, Short-range magnetic correlations and spin dynamics in the paramagnetic regime of $(Mn, Fe)_2(P, Si)$, Phys. Rev. B **94**, 014426 (2016).

[21] T. Faske, I. A Radulov, M. Hölzel, O. Gutfleisch, and W. Donner, Direct observation of paramagnetic spin fluctuations in $LaFe_{13-x}Si_x$, J. Phys.: Condens. Matter **32**, 115802 (2020).

[22] Z. Zhang, H. Zhou, R. Mole, C. Yu, Z. Zhang, X. Zhao, W. Ren, D. Yu, B. Li, F. Hu, B. Shen, and Z. Zhang, Intense ferromagnetic fluctuations preceding magnetoelastic first-order transitions in giant magnetocaloric $LaFe_{13-x}Si_x$, Phys. Rev. Mater. **5**, L071401 (2021).

[23] K. Morrison, J. J. Betouras, G. Venkat, R. A. Ewings, A. J. Caruana, K. P. Skokov, O. Gutfleisch, and L. F. Cohen, Emergence of a hidden magnetic phase in $LaFe_{11.8}Si_{1.2}$ investigated by inelastic neutron scattering as a function of magnetic field and temperature, Adv. Phys. Res. **3**, 2400008 (2024).

[24] R. J. C. Dixey, A. Wildes, P. W. Doheny, G. B. G. Stenning, and P. J. Saines, The magnetocaloric effect of the lanthanide fluorides: Using polarized neutron scattering to probe a magnetocaloric suitable for hydrogen liquefaction, APL Mater. **11**, 041126 (2023).

[25] R. Bouachraoui, Y. Ziat, Y. Sbai, O. El Rhazouani, F. Goumrhar, and L. Bahmad, The magnetocaloric and magnetic properties of the $MnFe_4Si_3$: Monte Carlo investigation, J. Alloys Compd. **809**, 151785 (2019).

[26] V. Singh, P. Bag, R Rawat, and R. Nath, Critical behavior and magnetocaloric effect across the magnetic transition in $Mn_{1+x}Fe_{4-x}Si_3$, Sci. Rep. **10**, 6981 (2020).

[27] H. Bińczycka, Z. Dimitrijević, B. Gajić, and A. Szytula, Atomic and magnetic structure of $Mn_{5-x}Fe_xSi_3$, Phys. Stat. Sol. (A) **19**, K13 (1973).

[28] We note that a combination of x-ray and neutron diffraction studies on single crystals proposes that $MnFe_4Si_3$ crystallizes in the lower symmetry hexagonal space group $P\bar{6}$ [29]. However, $P6_3/mcm$ can still be considered as an average structure of the low-symmetry space group $P\bar{6}$.

[29] P. Hering, K. Friese, J. Voigt, J. Persson, N. Aliouane, A. Grzechnik, A. Senyshyn, and T. Brückel, Structure, magnetism, and the magnetocaloric effect of $MnFe_4Si_3$ single crystals and powder samples, Chem. Mater. **27**, 7128 (2015).

[30] S. Raymond, N. Biniskos, K. Schmalzl, J. Persson, and T. Brückel, Total interference between nuclear and magnetovibrational one-phonon scattering cross sections, J. Phys.: Conf. Ser. **1316**, 012018 (2019).

[31] K. Schmalzl, W. Schmidt, S. Raymond, H. Feilbach, C. Mounier, B. Vettard, and T. Brückel, The upgrade of the cold neutron three-axis spectrometer IN12 at the ILL, Nucl. Instrum. Methods Phys. Res., Sect. A **819**, 89 (2016).

[32] G. L. Squires, *Introduction to the Theory of Thermal Neutron Scattering* (Cambridge University Press, Cambridge, 2012).

[33] *Neutron Scattering from Magnetic Materials*, 1st ed., edited by Tapan Chatterji (Elsevier, Amsterdam, 2005).

[34] J. W. Cable and R. M. Nicklow, Spin dynamics of Gd in an applied magnetic field, J. Phys.: Condens. Matter **1**, 7425 (1989).

[35] L. Rebelsky, P. Böni, S.M. Shapiro, H.G. Bohn, and W. Zinn, EuS above T_c: Spin wave excitations in magnetic fields, J. Magn. Magn. Mater. **84**, 201 (1990).

[36] N. Biniskos, S. Raymond, K. Schmalzl, A. Schneidewind, J. Voigt, R. Georgii, P. Hering, J. Persson, K. Friese, and T. Brückel, Erratum: Spin dynamics of the magnetocaloric compound $MnFe_4Si_3$ [Phys. Rev. B **96**, 104407 (2017)], Phys. Rev. B **98**, 219903(E) (2018).

[37] D.L. Huber, Effect of the pseudodipolar interaction on critical spin dynamics in cubic ferromagnets, Solid State Commun. **48**, 831 (1983).

[38] F. Mezei, Critical dynamics in isotropic ferromagnets, J. Magn. Magn. Mater. **45**, 67 (1984).

[39] P. Résibois and C. Piette, Temperature dependence of the linewidth in critical spin fluctuation, Phys. Rev. Lett. **24**, 514 (1970).

[40] In Ref. [9], the value A_0 for Ni_3Al is not given in the text. To obtain A_0, we used the data of Fig. 5 of the same reference and the exponent $z = 2.47$. Also note that T_C in Ni_3Al strongly depends on the exact concentration of Ni.

[41] P. Böni, H. A. Mook, J. L. Martínez, and G. Shirane, Comparison of the paramagnetic spin fluctuations in nickel with asymptotic renormalization-group theory, Phys. Rev. B **47**, 3171 (1993).

[42] P. Böni, J. L. Martínez, and J. M. Tranquada, Longitudinal spin fluctuations in nickel, Phys. Rev. B **43**, 575 (1991).

[43] H. Wada, A. Mitsuda, and K. Tanaka, Magnetic entropy change of itinerant electron metamagnetic system $Co(S_{1-x}Se_x)_2$, Phys. Rev. B **74**, 214407 (2006).
[44] S. K. Mishra, Heat capacity and magnetocaloric effect in $CoS_{1.84}Se_{0.16}$, J. Magn. Magn. Mater. **474**, 619 (2019).
[45] P. Arora, M. K. Chattopadhyay, and S. B. Roy, Magnetocaloric effect in MnSi, Appl. Phys. Lett. **91**, 062508 (2007).
[46] C. J. Glinka, V. J. Minkiewicz, and L. Passell, Small-angle critical neutron scattering from cobalt, Phys. Rev. B **16**, 4084 (1977).
[47] H. Schinz and F. Schwabl, Universality of the spin-wave frequency in ferromagnets below T_c, Phys. Rev. B **57**, 8456 (1998).
[48] F. Mezei, Role of spin-nonconserving forces in the critical dynamics of Fe at the Curie point, Phys. Rev. Lett. **49**, 1096 (1982).
[49] M. F. Collins, V. J. Minkiewicz, R. Nathans, L. Passell, and G. Shirane, Critical and spin-wave scattering of neutrons from iron, Phys. Rev. **179**, 417 (1969).
[50] P. Böni and G. Shirane, Paramagnetic neutron scattering from the Heisenberg ferromagnet EuO, Phys. Rev. B **33**, 3012 (1986).
[51] K. Ahn, A. O. Pecharsky, K. A. Gschneidner, Jr., and V. K. Pecharsky, Preparation, heat capacity, magnetic properties, and the magnetocaloric effect of EuO, J. Appl. Phys. **97**, 063901 (2005).
[52] D. X. Li, T. Yamamura, S. Nimori, Y. Homma, F. Honda, Y. Haga, and D. Aoki, Large reversible magnetocaloric effect in ferromagnetic semiconductor EuS, Solid State Commun. **193**, 6 (2014).
[53] N. Maraytta, Y. Skourski, J. Voigt, K. Friese, M.G. Herrmann, J. Persson, J. Wosnitza, S. M. Salman, and T. Brückel, Direct measurements of the magneto-caloric effect of $MnFe_4Si_3$ in pulsed magnetic fields, J. Alloys Compd. **805**, 1161 (2019).
[54] J. W. Lynn, Breakdown of dynamic scaling analysis in isotropic ferromagnets, Phys. Rev. Lett. **52**, 775 (1984).
[55] N. H. Dung, Z. Q. Ou, L. Caron, L. Zhang, D. T. Cam Thanh, G. A. de Wijs, R. A. de Groot, K. H. J. Buschow, and E. Brück, Mixed magnetism for refrigeration and energy conversion, Adv. Energy Mater. **1**, 1215 (2011).
[56] S. Komura, K. Tajima, H. Fujii, Y. Ishikawa, and T. Okamoto, Spin wave excitations in Fe_2P, J. Magn. Magn. Mater. **15–18**, 351 (1980).
[57] M. dos Santos Dias, N. Biniskos, F. J. dos Santos, K. Schmalzl, J. Persson, F. Bourdarot, N. Marzari, S. Blügel, T. Brückel, and S. Lounis, Topological magnons driven by the Dzyaloshinskii-Moriya interaction in the centrosymmetric ferromagnet Mn_5Ge_3, Nat. Commun. **14**, 7321 (2023).
[58] T. J. Williams, A. E. Taylor, A. D. Christianson, S. E. Hahn, R. S. Fishman, D. S. Parker, M. A. McGuire, B. C. Sales, and M. D. Lumsden, Extended magnetic exchange interactions in the high-temperature ferromagnet MnBi, Appl. Phys. Lett. **108**, 192403 (2016).
[59] P. Radhakrishna and J. W. Cable, Inelastic-neutron-scattering studies of spin-wave excitations in the pnictides MnSb and CrSb, Phys. Rev. B **54**, 11940 (1996).
[60] A. E. Taylor, T. Berlijn, S. E. Hahn, A. F. May, T. J. Williams, L. Poudel, S. Calder, R. S. Fishman, M. B. Stone, A. A. Aczel, H. B. Cao, M. D. Lumsden, and A. D. Christianson, Influence of interstitial Mn on magnetism in the room-temperature ferromagnet $Mn_{1+\delta}Sb$, Phys. Rev. B **91**, 224418 (2015).
[61] S. Yano, S. Itoh, T. Yokoo, S. Satoh, D. Kawana, Y. Kousaka, J. Akimitsu, and Y. Endoh, Magnetic excitations in ferromagnetic phase of MnP, J. Magn. Magn. Mater. **347**, 33 (2013).
[62] W. F. Brinkman and S. Engelsberg, Spin-fluctuation contributions to the specific heat, Phys. Rev. **169**, 417 (1968).
[63] G.G. Lonzarich, The magnetic equation of state and heat capacity in weak itinerant ferromagnets, J. Magn. Magn. Mater. **54**, 612 (1986).
[64] S. M. Hayden, R. Doubble, G. Aeppli, T. G. Perring, and E. Fawcett, Strongly enhanced magnetic excitations near the quantum critical point of $Cr_{1-x}V_x$ and why strong exchange enhancement need not imply heavy fermion behavior, Phys. Rev. Lett. **84**, 999 (2000).
[65] A. P. Murani, A. Krimmel, J. R. Stewart, M. Smith, P. Strobel, A. Loidl, and A. Ibarra-Palos, The paramagnetic spectral response from LiV_2O_4, J. Phys.: Condens. Matter **16**, S607 (2004).
[66] C. Lester, S. Ramos, R. S. Perry, T. P. Croft, M. Laver, R. I. Bewley, T. Guidi, A. Hiess, A. Wildes, E. M. Forgan, and S. M. Hayden, Magnetic-field-controlled spin fluctuations and quantum criticality in $Sr_3Ru_2O_7$, Nat. Commun. **12**, 5798 (2021).
[67] A. V. Lazuta, S. V. Maleyev, and B. P. Toperverg, Critical dynamics of ferromagnets above T_C in a magnetic field, Zh. Eksp. Teor. Fiz. **81**, 2095 (1981) [Sov. Phys. JETP **54**, 1113 (1981)].
[68] https://doi.ill.fr/10.5291/ILL-DATA.4-01-1773 (2023).
[69] https://doi.ill.fr/10.5291/ILL-DATA.INTER-576 (2023).
[70] https://doi.ill.fr/10.5291/ILL-DATA.CRG-2579 (2019).